Ultra-sensitive wavefront measurement using a Hartmann sensor

Aidan F. Brooks, Thu-Lan Kelly, Peter J. Veitch, and Jesper Munch

The University of Adelaide, Adelaide, SA, 5005

aidan.brooks@adelaide.edu.au

Abstract: We describe a Hartmann sensor with a sensitivity of $\lambda/15,500$ at $\lambda = 820\,\text{nm}$. We also demonstrate its application to the measurement of an ultra small change in wavefront and show that the result agrees with that expected to within $\lambda/3,300$.

OCIS codes: (120.4640) Optical instruments; (010.7350) Wave-front sensing; (350.4800) Optical standards and testing

References and links

1. J. Hartmann, "Bemerkungen uber den Bau und die Justirung von Spektrographen," Zt. Instrumentenkd. **20,** 47 (1900).
2. T. L. Kelly, P. J. Veitch, A. F. Brooks and J. Munch, "A differential Hartmann wavefront sensor for accurate and precise optical testing," Appl. Opt. **46,** 861–866 (2007).
3. C. Castellini, F. Francini and B. Tiribilli, "Hartmann test modification for measuring ophthalmic progressive lenses," Appl. Opt. **33,** 4120 (1994).
4. F. Roddier, ed., *Adaptive Optics in Astronomy* (Cambridge U. Press, Cambridge, England, 1999).
5. J. D. Mansell, J. Hennawi, E. K. Gustafson, M. M. Fejer, R. L. Byer, D. Clubley, S. Yoshida and D. H. Reitze, "Evaluating the effect of transmissive optic thermal lensing on laser beam quality with a Shack-Hartmann wavefront sensor," Appl. Opt. **40,** 366–374 (2001).
6. R. Lawrence, D. Ottaway, M. Zucker and P. Fritchel, "Active correction of thermal lensing through external radiative thermal actuation," Opt. Lett. **22,** 2635-2637 (2004).
7. M. Smith and P. Willems, "Auxiliary Optics Support System Conceptual Design Document, Vol. 1: Thermal Compensation System," (2006), http://www.ligo.caltech.edu/docs/T/T060083-00/T060083-00.pdf.
8. A. Chernyshov, U. Sterr, F. Riehle, J. Helmcke and J. Pfund, "Calibration of a Shack-Hartmann sensor for absolute measurements of wavefronts," Appl. Opt. **44,** 6419–6425 (2005).
9. J. L. Rayces, "Exact Relation between Wave Aberration and Ray Aberration," Opt. Acta. **11,** 85–88 (1964).
10. W. H. Southwell, "Wave-front estimation from wave-front slope measurements," J. Opt. Soc. Am. **70,** 998–1006 (1980).
11. P. Mercere, P. Zeitoun, M. Idir, S. Le Pape, D. Douillet, X. Levecq, G. Dovillaire, S. Boucourt, K. A. Goldberg, P. P. Naullleau and S. Rekawa, "Hartmann wave-front measurement at 13.4 nm with $\lambda_{EUV}/120$ accuracy," Opt. Lett. **28,** 1534–1536 (2003).
12. A. Poteomkin, N. Andreev, I. Ivanov, E. Khazanov, A. Shaykin, and V. Zelenogorsky, "Use of a scanning Hartmann sensor for measurement of thermal lensing in TGG crystal," Proc. SPIE **4970,** 10–21 (2003).
13. M. Kasper, D. Looze, S. Hippler, R. Davies and A. Glindemann, "Increasing the sensitivity of a Shack-Hartmann sensor," in Proceedings of the Canterbury Conference on Wavefront sensing and its applications, Canterbury (1999), http://mpia-hd.mpg.de/ALFA/PAPERS/canterbury99MEK.pdf.

1. Introduction

Hartmann wavefront sensors, first described in 1904 [1], and particularly the Shack-Hartmann derivatives, have enjoyed a recent surge of popularity due to improvements in the speed, quality and size of CCD arrays. They are currently used for a variety of applications, including lens metrology [2], ophthalmology [3], adaptive optics [4] and the measurement of thermal lensing

#83447 - $15.00 USD Received 25 May 2007; revised 25 Jul 2007; accepted 31 Jul 2007; published 2 Aug 2007

[5] [6]. The measurement of wavefront distortion induced by absorption in the optics of advanced gravitational wave interferometers is a particularly demanding application, requiring a sensitivity equivalent to at least $\lambda/600$ at $\lambda = 820\,\mathrm{nm}$ [7].

The type of Hartmann sensor used for an application is usually dictated by the intensity of the available light source. Shack-Hartmann sensors use micro-lens arrays to sample the wavefront and thus optimize the light collection efficiency but they are susceptible to imperfections in the micro-lens array [8]. While the effect of these imperfections can be partially reduced by calibration of the system, they can't be fully removed [8] as the resulting aberration of the calibrating wavefront by the imperfection is, in general, different from that imposed on an unknown wavefront. A Hartmann wavefront sensor, by contrast, samples the wavefront, *W*, using an opaque plate containing an array of holes, the Hartmann plate, as shown schematically in part of Fig. 1. It is therefore less light efficient, but it is simple to optimize and, as shown here, has ultra-high sensitivity and accuracy when measuring wavefront changes.

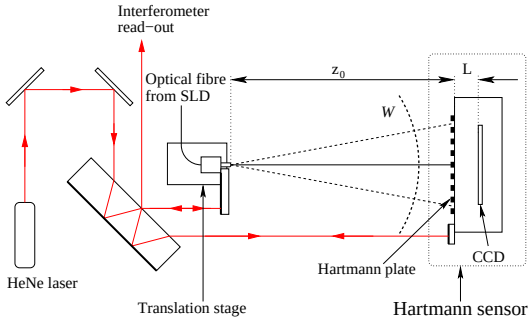

Fig. 1. A schematic of the Hartmann wavefront sensor and the system used to test it. The sensor consists of a Hartmann plate mounted a distance L from a CCD. It was illuminated by a wavefront *W* emitted from a fiber-coupled super luminescent diode (SLD), the free end of the which was mounted on a micrometer-controlled translation stage.

The rays created by the Hartmann plate propagate normal to the incident wavefront *W* to the active surface of a CCD where they produce an array of spots. If the local slope of the wavefront changes then the positions of the spots will change. Dividing the transverse displacement of each spot by the 'lever-arm' propagation length L yields the gradient of the wavefront change at each hole (see [9] for example), and the wavefront change, ΔW, can be determined by numerically integrating this gradient field [10]. While knowledge of the initial wavefront would then enable the new wavefront to be calculated, in this paper we do not make any assumptions about the initial wavefront but rather consider only the change, ΔW, in the wavefront as required for the measurement of thermal lensing in gravitational wave interferometers.

The position of each spot is specified by its centroid, the precision of which is maximized by ensuring that each spot consists of a large number of pixels and that each pixel acquires a large number of photoelectrons in the available integration time. This minimizes the effects of dark current, CCD read-out noise, non-uniformity in pixel response and photoelectron shot noise. Since Hartmann wavefront sensors naturally provide large spot sizes, they should be able to provide high sensitivity measurements of wavefront changes. Indeed, a Hartmann sensor that has a reproducibility (sensitivity) of $\lambda/1500$ at $\lambda = 13.4\,\mathrm{nm}$ [11] and a scanning Hartmann sensor that has a sensitivity of $\lambda/500$ at $\lambda = 1064\,\mathrm{nm}$ [12] have been reported. The accuracy of the scanning Hartmann sensor was estimated to be $\lambda/50$ at $\lambda = 1064\,\mathrm{nm}$. In this paper, we describe an investigation of the optimization of a Hartmann wavefront sensor (H-WFS) and demonstrate significant improvements in the sensitivity and accuracy of this type of sensor.

#83447 - $15.00 USD Received 25 May 2007; revised 25 Jul 2007; accepted 31 Jul 2007; published 2 Aug 2007

2. Hartmann wavefront sensor

The camera used in our sensor is a 12-bit digitized, 1024×1024 pixel CCD camera that has a nominal dynamic range of 66 dB (11 bits) and a nominal pixel spacing of $12\,\mu$m. The actual average pixel spacing was measured by translating the camera sideways using a micrometer-controlled translation stage and observing the displacement on the CCD of a fixed diffraction pattern, yielding a value of $11.975 \pm 0.005\,\mu$m.

The Hartmann plate was made from $50\,\mu$m thick brass plate into which $150\,\mu$m diameter holes in a uniform hexagonal-close-packed array spaced $430\,\mu$m apart were laser drilled, yielding about 900 holes over the 12.2 mm $\times$ 12.2 mm CCD. It was mounted on the body of the camera and the distance between the plate and the active surface of the CCD, the lever arm L, was calibrated by illuminating the sensor with two laser beams separated by a precisely measured angle and measuring the average displacement between the two spot patterns, giving $\mathrm{L} = 10.43 \pm 0.02\,$mm. The hole diameter, pitch, pattern and value of L were optimized to ensure that cross-talk between neighbouring spots was negligible while maintaining sensitivity.

A weighted centroiding algorithm was used to determine the spot positions [13]: $x_c = \sum_i p_i^2 x_i / \sum_i p_i^2$ and $y_c = \sum_i p_i^2 y_i / \sum_i p_i^2$ where p_i is the digital number, directly proportional to the number of photoelectrons, and x_i and y_i are the coordinates of the i^{th} pixel. The summation range of the algorithm was adjusted to minimize the variance in the centroids. In practice, this meant using only pixels within a box that was 15 pixels square, which is 10% larger than the hole diameter. Simulations indicate that cross-talk due to diffraction should introduce a systematic error of less than 0.1% for the defocus measurement discussed in this paper.

All measurements reported here were recorded after a 3 hour warm-up period to reduce the effects of thermal expansion of the sensor. However, there was a residual 0.5 mHz oscillation in the output of the H-WFS due to a periodic variation in the temperature of the sensor with an amplitude of 150 mK, caused by the cycling of the room temperature. The magnitude of the oscillation is consistent with thermal expansion of the Hartmann plate.

The H-WFS was tested using the system shown in Fig. 1, in which it was illuminated by light emitted from an optical fiber with a $50\,\mu$m core and 0.36 NA that was coupled to an 820 nm super-luminescent diode, which had a full-width-half-maximum coherence length of about $5\,\mu$m. The optical table on which the H-WFS and its test system were mounted was enclosed to reduced air currents A Michelson interferometer was used to measure changes in the distance, z_0, between the light source and the H-WFS with a precision of 50 nm.

3. Results

The statistics of the noise in the H-WFS were investigated by illuminating the CCD with the output from the fiber at three different intensity levels. A short integration time was used to ensure that the dark current was negligible. We observed that the fluctuation, Δp, in the digital number, p, in a pixel was well described by $\Delta p \propto p^{0.5}$, proving the noise has Poissonian statistics. A relative fluctuation of 0.25% was obtained for the maximum digital number (4095), indicating a maximum photoelectron count of approximately 1.6×10^5, which is similar to the specified electron well depth of each pixel, confirming that the dominant noise is photoelectron shot noise.

Numerical simulation predicts that the RMS uncertainty in the centroid position due to photoelectron shot noise in a single Hartmann image should be about 0.25% of a pixel, or about 30 nm, if the brightest pixel in each spot is full. If the noise in sequential Hartmann images is uncorrelated then the RMS error in the displacement of a centroid, $\sigma_{\Delta y}$, will be a factor of $2^{1/2}$ larger. The RMS wavefront difference between *adjacent holes*, $\sigma_{\Delta W}$, is given by $\sigma_{\Delta W} = \sigma_{\Delta y} h_p / L$, where h_p is the spacing between adjacent holes in the Hartmann plate. If the noise in neighbouring centroids is not spatially correlated then the RMS wavefront error across *all holes* can be

#83447 - $15.00 USD Received 25 May 2007; revised 25 Jul 2007; accepted 31 Jul 2007; published 2 Aug 2007

determined using $C_{\mathrm{pd}}^{1/2} \times \sigma_{\Delta W}$, where C_{pd} is the noise coefficient developed by Southwell [10], which is dependent on the number, N_{holes}, and arrangement of holes. More generally, however, the RMS wavefront error is determined from the map produced by numerically integrating the gradient field [10].

The RMS wavefront error was measured using the system shown in Fig. 1 while keeping z_0 constant. Spot centroids were calculated for consecutive Hartmann images separated in time by 15 s and the average prism in each image was removed. These zero-prism centroids were used to calculate the error in the wavefront change. A typical map of the wavefront change, which has an RMS error of $\lambda/1450$, is shown in Fig. 2. The RMS error for these maps varied between $\lambda/1000$ and $\lambda/2000$ which is consistent with the shot noise limit and $C_{\mathrm{pd}} = 0.2$, calculated for $N_{\mathrm{holes}} = 263$ used in this example.

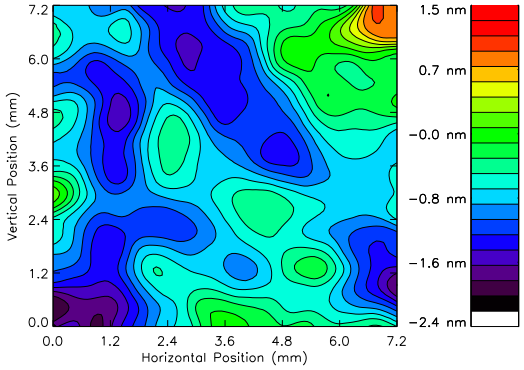

Fig. 2. Measured single-frame wavefront error map over a 7.2 mm × 7.2 mm region.

If the statistical characteristics of the noise do not vary with time then the wavefront error should be reduced by averaging over multiple Hartmann images. To test this, we recorded a sequence of 2000 Hartmann images at 30 images/second and removed the global prism from each image. A set of reference centroids was then calculated by averaging over $N_{\mathrm{ref}} = 1000$ images, consisting of the first and last 500 images. The central 1000 images were used to calculate sets of centroids averaged over N_{avg} images, where $N_{\mathrm{avg}} = 1, \ldots, 990$. This process ensured that the reference and average centroids were statistically independent. The resulting $\sigma_{\Delta W}$ are plotted in Fig. 3, showing that the minimum $\sigma_{\Delta W} \approx \lambda/15,500$.

The result of a numerical simulation that assumes stationary random noise and in which the only free parameter is the $N_{\mathrm{avg}} = 1$ error is also plotted in Fig. 3. For small N_{avg}, the error decreases as $N_{\mathrm{avg}}^{1/2}$, as expected, and it asymptotically approaches a value that is a factor N_{ref} times smaller than the $N_{\mathrm{avg}} = 1$, the limit due to the noise in the reference centroids. Note the good agreement between the measurement and the numerical simulation except for $N_{\mathrm{avg}} > 200$ where the measured error is slightly larger than that predicted.

The RMS wavefront error across all holes for $N_{\mathrm{avg}} = 990$ was $\lambda/15,500$, which is larger than the value $C_{\mathrm{pd}}^{1/2} \times \sigma_{\Delta W} = \lambda/21,000$ predicted using the simulated data and the Southwell noise coefficient appropriate for this measurement. These discrepancies are probably due to the effect of the low-frequency temperature fluctuation described above.

The ability of the H-WFS to measure a small known (modal) change in the wavefront, ΔW, was demonstrated by translating the fiber light source. As shown in Fig. 4, translating the source a distance Δz from an initial position z_0 displaces the spot on the CCD by $\Delta y(h)$, assuming that the change in the slope of each wavefront across the hole is small. The expected local gradient

#83447 - $15.00 USD Received 25 May 2007; revised 25 Jul 2007; accepted 31 Jul 2007; published 2 Aug 2007

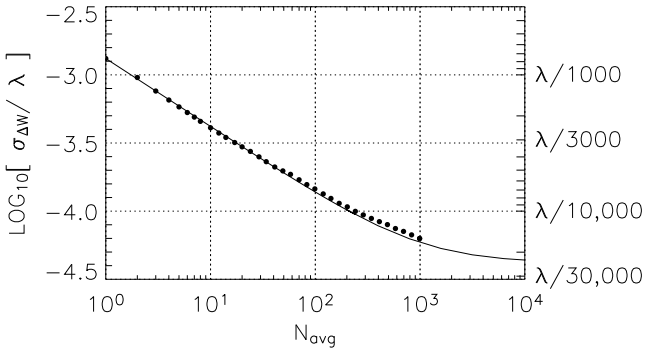

Fig. 3. The improvement in H-WFS sensitivity due to averaging over N_{avg} Hartmann images. The solid curve shows the improvement predicted by a numerical simulation assuming only random, stationary noise in the spot centroids.

of the wavefront change can then be calculated using

$$\frac{\partial(\Delta W)}{\partial h} = \frac{\Delta y}{L} = \frac{\Delta z y_0}{(z_0 - \Delta z)(z_0 + L)} = \frac{\Delta z h}{(z_0 - \Delta z) z_0} = Sh \tag{1}$$

where h is the position of the hole in the Hartmann plate, S is the primary aberration defocus and we have considered only one dimension for clarity.

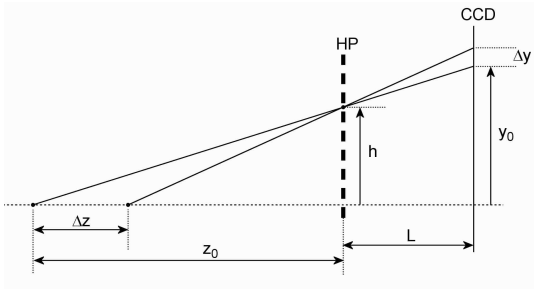

Fig. 4. Schematic diagram showing the displacement of the Hartmann spot on the CCD due to a change in the distance between the fiber end and the H-WFS.

Unfortunately, the 0.5 mHz oscillation in the output of the H-WFS resulted in a synchronous oscillation in the calculated defocus. We therefore recorded Hartmann images continuously at 40 Hz and translated the fibre by about 10 μm every 5-10 minutes. The translation that occurred nearest a turning point of the 0.5 mHz oscillation was then selected for analysis, as this ensured that the average temperature of the H-WFS was the same before and after the translation. Plots of the local gradient of the wavefront change for $\Delta z = 9.60 \pm 0.05\,\mu$m, versus the transverse position, y_0, of each spot are shown in Fig. 5. They show a linear relationship between the local gradient and transverse position as predicted by Eq. 1, and the improvement in sensitivity due to averaging.

The defocus due to the source translation can be calculated using the slope, m, of the line-of-best-fit to this data and $S = m(z_0 + L)/z_0$. The defocus for the 1-image and 5000-image averages are $-1.3 \pm 0.2 \times 10^{-3}\,\text{m}^{-1}$ and $-1.159 \pm 0.007 \times 10^{-3}\,\text{m}^{-1}$ at 95% confidence level. The uncertainty in S when averaged over 5000 images is equivalent to an uncertainty in the wavefront sag of 0.1 nm $(\lambda/9300)$ over the CCD aperture (≈ 10 mm), which is roughly twice the

#83447 - $15.00 USD Received 25 May 2007; revised 25 Jul 2007; accepted 31 Jul 2007; published 2 Aug 2007

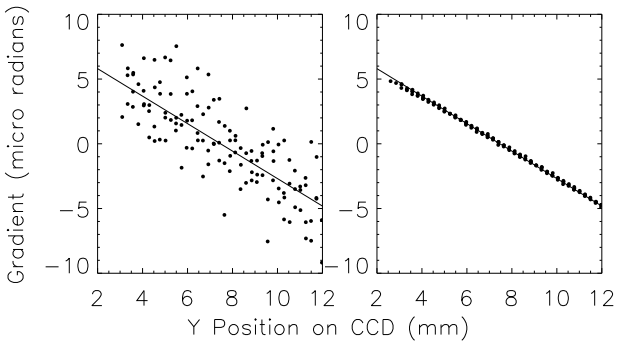

Fig. 5. Measured local gradient of the wavefront change versus spot position at the CCD, y_0, due to translation of the fiber light source, averaged over (left) 1 and (right) 5000 Hartmann images.

previously measured $\lambda/15,500$ due probably to the non-stationary noise during the extended acquistion time.

The accuracy of the defocus measurement can be determined by comparing the measured defocus with that predicted using Eq. 1, but this comparison requires an accurate measurement of z_0. The distance between the source and the H-WFS was determined by exploiting the non-linear dependence of the local gradient on Δz: analyzing Hartmann images recorded with large Δz and determining the value of z_0 that would produce the best agreement between the measured local gradient and that predicted by Eq. 1. With this approach, we found $z_0 = 91.7 \pm 0.2$ mm, giving an expected defocus of $-1.14 \pm 0.01 \times 10^{-3}\mathrm{m}^{-1}$, which differs from the measurement by about 1.7%. This error is equivalent to $\lambda/3,300$ and could be explained by a change in average temperature of the H-WFS of order 10 mK.

4. Conclusion

We have demonstrated that the H-WFS can measure changes in a wavefront with a single-frame sensitivity of $\lambda/1450$, which is primarily limited by shot noise. We have also shown that the sensitivity can be improved to $\lambda/15,500$ by averaging multiple Hartmann images. Finally, we demonstrated its application to the measurement of a small wavefront change due to defocus with a precision of $7 \times 10^{-6}\,\mathrm{m}^{-1}$ and established that the sensor is accurate to within about $2.0 \times 10^{-5}\,\mathrm{m}^{-1}$.

Together with the simplicity of the H-WFS, these results show that it is ideal for high precision and high accuracy measurement of wavefront changes, and represent a large improvement in the state-of-the-art. The H-WFS clearly exceeds the requirement for the measurement of absorption-induced wavefront distortion in advanced gravitational wave interferometers.

Acknowledgments

We acknowledge support from the Australian Research Council.

#83447 - $15.00 USD Received 25 May 2007; revised 25 Jul 2007; accepted 31 Jul 2007; published 2 Aug 2007